Materials Today Bio 29 (2024) 101343

Contents lists available at ScienceDirect

Materials Today Bio

journal homepage: www.journals.elsevier.com/materials-today-bio

Idarubicin-loaded degradable hydrogel for TACE therapy enhances anti-tumor immunity in hepatocellular carcinoma

Xiaokai Zhang [a,b,1], Xiujiao Deng [c,d,1], Jizhou Tan [e,1], Haikuan Liu [b], Hong Zhang [f], Chengzhi Li [c], Qingjun Li [a], Jinxue Zhou [a,**], Zeyu Xiao [c,*], Jiaping Li [b,***]

[a] Department of Hepatobiliopancreatic Surgery, Affiliated Cancer Hospital of Zhengzhou University, Henan Cancer Hospital, Zhengzhou 450003, China
[b] Department of Interventional Oncology, The First Affiliated Hospital, Sun Yat-sen University, Guangzhou 510080, China
[c] The Guangzhou Key Laboratory of Molecular and Functional Imaging for Clinical Translation, Department of Radiology and Nuclear Medicine, The First Affiliated Hospital of Jinan University, Guangzhou 510632, China
[d] Department of Pharmacy, The First Affiliated Hospital of Jinan University, Guangzhou, 510632, China
[e] Department of Stomatology, The First Affiliated Hospital, Sun Yat-sen University, Guangzhou 510080, China
[f] Department of Interventional Radiology and Vascular Surgery, The Sixth Affiliated Hospital of Jinan University, Dongguan 523067, China

ARTICLE INFO

Keywords:
Hepatocellular carcinoma
Transarterial chemoembolization
Immunogenic cell death
Idarubicin
Composite hydrogel

ABSTRACT

Hepatocellular carcinoma (HCC) is a common and deadly cancer, often diagnosed at advanced stages, limiting surgical options. Transcatheter arterial chemoembolization (TACE) is a primary treatment for inoperable and involves the use of drug-eluting microspheres to slowly release chemotherapy drugs. However, patient responses to TACE vary, with some experiencing tumor progression and recurrence. Traditional TACE uses agents like oil-based drug emulsions and polyvinyl alcohol particles, which can permanently block blood vessels and increase tumor hypoxia. Additionally, TACE can suppress the immune system by reducing immune cell numbers and function, contributing to poor treatment outcomes. New approaches, like TACE using degradable starch microspheres and hydrogel-based materials, offer the potential to create different tumor environments that could improve both safety and efficacy. In our research, we developed a composite hydrogel (IF@Gel) made of Poloxamer-407 gel and Fe_3O_4 nanoparticles, loaded with idarubicin, to use as an embolic material for TACE in a rat model of orthotopic HCC. We observed promising therapeutic effects and investigated the impact on the tumor immune microenvironment, focusing on the role of immunogenic cell death (ICD). The composite hydrogel demonstrated excellent potential as an embolic material for TACE, and IF@Gel-based TACE demonstrated significant efficacy in rat HCC. Furthermore, our findings highlight the potential synergistic effects of ICD with anti-PD-L1 therapy, providing new insights into HCC treatment strategies. This study aims to provide improved treatment options for HCC and to deepen our understanding of the mechanisms of TACE and tumor environment regulation.

Abbreviations: HCC, Hepatocellular carcinoma; TACE, Transcatheter arterial chemoembolization; c-TACE, conventional TACE; PVA, polyvinyl alcohol; DEB-TACE, drug-eluting beads-TACE; VEGF, vascular endothelial growth factor; DSM-TACE, degradable starch microspheres TACE; ICD, immunogenic cell death; SEM, scanning electron microscope; MRI, magnetic resonance imaging; DSA, digital subtraction angiography; DWI, diffusion-weighted imaging; T2WI, T2-weighted imaging; HE staining, hematoxylin-eosin staining; ALT, alanine aminotransferase; AST, aspartate transaminase; CREA, creatinine; BUN, blood urea nitrogen; TUNEL, terminal deoxynucleotidyl transferase dUTP Nick-End labeling; CTLs, cytotoxic T lymphocytes; NK, natural killer; GO, gene ontology; KEGG, kyoto encyclopedia of genes and genomes; DDR, DNA damage response; HMGB1, high mobility group box-1 protein; CRT, calreticulin; ICI, immune checkpoint inhibitor.

* Corresponding author.
** Corresponding author.
*** Corresponding author.
E-mail addresses: zhoujx888@126.com (J. Zhou), zeyuxiao@jnu.edu.cn (Z. Xiao), lijiap@mail.sysu.edu.cn (J. Li).
[1] These authors contributed equally to this work.

https://doi.org/10.1016/j.mtbio.2024.101343
Received 23 August 2024; Received in revised form 22 October 2024; Accepted 14 November 2024
Available online 23 November 2024
2590-0064/© 2024 Published by Elsevier Ltd. This is an open access article under the CC BY-NC-ND license (http://creativecommons.org/licenses/by-nc-nd/4.0/).

1. Introduction

Hepatocellular carcinoma (HCC), as a clinically prevalent malignant tumor, has a consistently high incidence rate and has become one of the leading causes of cancer-related deaths worldwide [1]. Unfortunately, HCC is often diagnosed at advanced stages, depriving many patients of the optimal window for surgical resection [2]. To address this clinical challenge, transcatheter arterial chemoembolization (TACE) has emerged as a frontline therapeutic approach recommended for HCC patients ineligible for surgical resection [3]. By utilizing drug-eluting microspheres and other embolic agents, TACE achieves significant application in HCC treatment through the slow release of chemotherapeutic drugs [4]. However, recent studies have highlighted variations in patient responses to TACE, with some experiencing tumor progression, recurrence, and metastasis post-treatment [5]. This highlights an urgent need for further research into the mechanisms contributing to poor prognoses following TACE, to develop more effective treatment strategies.

Common embolic agents used in clinical practice include conventional TACE (c-TACE), which involves chemotherapeutic drug emulsions based on iodized oil, often supplemented with gelatin sponge particles, blank microspheres, or polyvinyl alcohol (PVA) particles [6]. Another method is drug-eluting beads-TACE (DEB-TACE) [7], both of which can lead to permanent occlusion of the embolized hepatic arteries, worsening the tumor's hypoxic environment after treatment [8]. While embolization-induced hypoxia can trigger apoptosis and necrosis in the majority of tumor cells, a subset of residual cells may exhibit heightened malignancy and resistance to conventional chemotherapy, thereby contributing to tumor progression post-TACE [9,10]. This effect is primarily due to prolonged ischemia, which can stimulate the production of vascular endothelial growth factor (VEGF), promoting the development of new tumor vasculature [11]. In addition, poor outcomes following TACE may be related to the tumor immune microenvironment, which has been shown to play an important role in HCC recurrence [12]. Our team has demonstrated that conventional TACE embolic agents can reduce the number and function of immune cells, resulting in significant immunosuppression [13]. Therefore, addressing hypoxia and ameliorating the immunosuppressive microenvironment to eliminate residual tumor cells emerge as crucial avenues for advancing the development of high-performance TACE materials.

Recent research suggests that utilizing novel embolic materials or adjusting the intensity of embolization—such as with degradable starch microspheres TACE (DSM-TACE) and hydrogel-based TACE—not only ensures safety and efficacy but also creates tumor microenvironments distinct from those resulting from traditional TACE [14–16]. While these improvements are generally viewed positively, the precise mechanisms driving these microenvironmental changes require further investigation.

Moreover, the chemotherapeutic agents commonly used for HCC, primarily platinum-based and anthracycline-based drugs (e.g., cisplatin, oxaliplatin, doxorubicin, epirubicin, and idarubicin), are considered inducers of immunogenic cell death (ICD) [17,18]. ICD is believed to be a mechanism for activating the immune system, promoting the presentation of tumor antigens, and activating immune cells, thus potentially playing a crucial role in enhancing the immune effects of TACE treatment [19]. More encouragingly, a synergistic effect between ICD and anti-PD-L1 therapy has been reported, which may further decrease the formation of an immunosuppressive microenvironment and reduce the risk of tumor recurrence and metastasis [16,20–22].

Based on these findings, we have focused on exploring the potential of degradable hydrogels for treating HCC. We selected a facilely prepared, degradable Poloxamer-407-based composite hydrogel, loaded with idarubicin, as the TACE treatment approach. In this study, we will evaluate the therapeutic efficacy of this treatment in an SD rat model of HCC and investigate changes in the tumor immune microenvironment following treatment. Additionally, we will study the potential mechanisms of action involving ICD (Scheme 1). Through this research, we aim

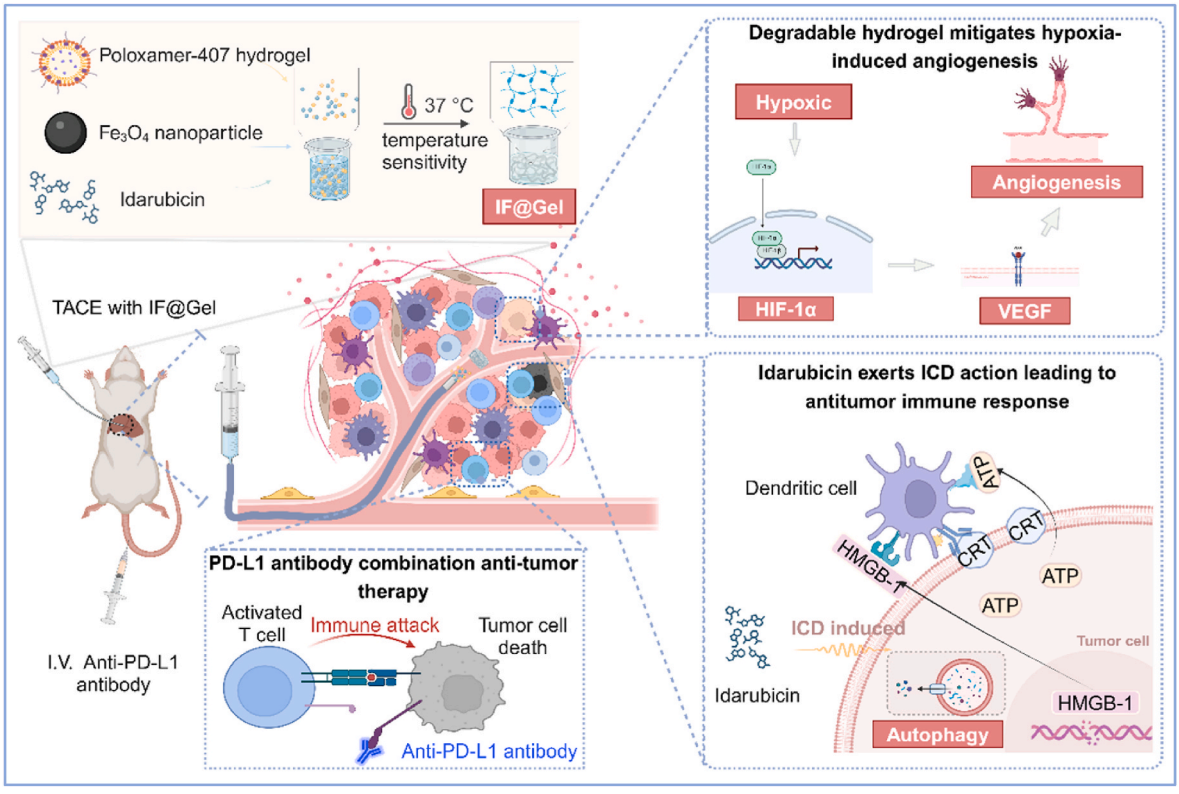

Scheme 1. Idarubicin-loaded degradable hydrogel for TACE therapy alleviates hypoxia-induced angiogenesis and exerts anti-immune effects on hepatocellular carcinoma by activating immunogenic cell death and synergizing with anti-PD-L1.

to provide more effective treatment options for HCC patients while offering new insights and theoretical foundations for understanding TACE mechanisms and tumor microenvironment regulation.

2. Materials and methods

2.1. Human tissue samples

From 2019 to 2021, surgical samples for transcriptome sequencing were collected from five treatment-naive primary patients (PT) and five patients (TT) who underwent TACE treatment at The First Affiliated Hospital of Sun Yat-sen University. PT samples were obtained via needle biopsy, while TT samples were obtained through surgical resection. All patients in the TT group received only DEB-TACE loaded with doxorubicin, without any prior targeted therapy or immunotherapy. Informed consent was obtained from all patients for the collection of their clinical information and tissue samples. The research procedures were conducted by protocols approved by the ethics committee of The First Affiliated Hospital of Sun Yat-sen University (2018 [43], 2021[204]). Specific patient information and the operational methods of transcriptome sequencing have been detailed in the published article [13] and will not be reiterated here.

2.2. Preparation of hydrogels

Preparation of Poloxamer- 407 hydrogels: Weigh 2g of Poloxamer-407 particles and put them into a centrifuge tube containing 10 ml of sterilized deionized water. Mix thoroughly and refrigerate at 4 °C overnight to form a 20 % Poloxamer-407 hydrogel.

Preparation of Fe_3O_4@Gel composite hydrogel: Fe_3O_4@Gel was made by mixing 1 mL of Fe_3O_4 nanoparticles (1 mg/mL) with the Ploxamer-407 mentioned above hydrogel at a volume ratio of 1:10 with sufficient shaking.

Preparation of IF@Gel composite hydrogel: Dissolve Idarubicin hydrochloride powder in sterilized deionized water to make a storage solution of 10 mg/mL and keep at 4 °C. Add this stock solution to Fe_3O_4@Gel composite hydrogel solution to bring the final drug concentration to 1 mg/mL.

2.3. Characterization of hydrogels

Poloxamer-407 hydrogel and IF@Gel composite hydrogel were placed in a rheometer (Thermo Fisher, USA) to assess their viscosity changes with temperature and compare the mechanical strengths of the two gels. The hydrogel samples, with a thickness of 1 mm, were placed between the rows of plates, with the gap adjusted to 1 mm. The relationship between the energy storage modulus (G') and loss modulus (G") with the temperature (10–45 °C) was determined, with the test conducted at 37 °C.

The structures of Poloxamer-407 hydrogel and IF@Gel composite gel were examined using a scanning electron microscope (SEM) (Carl Zeiss, Germany), and the structures of Fe_3O_4 nanoparticles were analyzed using a transmission electron microscope (Carl Zeiss, Germany).

2.4. In vitro and in vivo degradation of hydrogels

In vitro, degradation experiments: Poloxamer-407 hydrogel and IF@Gel composite gel were placed into a specimen bottle filled with PBS at 37 °C. Their degradation over time was monitored, and photographs were taken to document the changes.

In vivo degradation experiment: IF@Gel composite gel was injected into the subcutaneous of C57BL/6 mice through a syringe. The mice were euthanized at 0 h, 4 h, 12 h, and 24 h post-injection. The skin was then removed to observe the diffusion and degradation of the subcutaneous gel, and photographs were taken for documentation.

2.5. Cell lines and cell culture

The rat hepatocellular carcinoma N1S1 cell line, a generous donation from Prof. Minhao Wu at Sun Yat-sen University, was used in this study. N1S1 cells were cultured in DMEM (Gibco, USA) containing 10 % fetal bovine and 1 % penicillin-streptomycin in culture flasks of 25 cm^2 and maintained in a humidified incubator with 5 % CO_2 at 37 °C.

2.6. Experimental animals

Twelve-week-old male SD rats (weight range 300~350g) and 4-week-old male C57BL/6 mice were purchased from the Laboratory Animal Center of Sun Yat-sen University. They passed the ethical application (approval number: 2021000985).

2.7. Animal model construction

Rat in orthotopic HCC model: SD rats were subjected to a 12-h fasting period followed by a 6-h water deprivation. Anesthesia was induced using 3 % isoflurane inhalation. Rats were immobilized in the supine position on the operating table, and a longitudinal incision approximately 1.5 cm in length was made in the midline of the abdomen, just below the xiphoid process. The abdominal wall was gently expanded using a retractor to expose the liver's middle and left lateral lobes. A 200 μL suspension of N1S1 cells (2×10^6 cells) was aspirated using an insulin needle and injected slowly into the hepatic parenchyma of the left lateral lobe, forming a transparent, rounded bulge at the injection site. The puncture site was pressed with a cotton swab to prevent bleeding and leakage of tumor cell suspension. After confirming the absence of active bleeding in the abdominal cavity, the abdominal wall was sutured, and anesthesia was discontinued following alcohol sterilization. After recovery, the rats were allowed to resume their regular diet, and intramuscular penicillin (200,000 units) was administered for three consecutive days post-surgery.

Rat model of in orthotopic HCC combined with abdominal metastasis: Following the procedure above for constructing the in orthotopic HCC model, a 200 μL suspension of N1S1 cells (2×10^6 cells) was inoculated into the abdominal cavity to induce abdominal metastasis.

2.8. TAE/TACE therapy

SD rats harboring in orthotopic HCC underwent a 12-h fast and 6-h water deprivation before being anesthetized with 3 % isoflurane. Positioned supine on the operating table, their abdomen was incised to about 4~5 cm and gently spread open to expose the entire abdominal cavity. Surgical procedures were performed using a microscope to lift the liver's middle and left outer lobes and clip the hepatogastric ligament. The common hepatic artery was clamped, and the gastroduodenal artery was ligated. A microcatheter was inserted into the gastroduodenal artery, advanced to the hepatic artery, and connected to a syringe for therapy or contrast agent injection. After catheter removal, the incision was sutured, and postoperative penicillin was administered for three days to prevent infection.

TAE/TACE regimen for orthotopic HCC in rats. 25 rats were divided into 5 groups, (1) Control group: no treatment, (2) Poloxamer-407 TAE Group: 200 μL of 20 % Poloxamer-407 hydrogel was injected via TAE, (3) Fe_3O_4@Gel TAE group: 200 μL of Fe_3O_4@ Gel composite hydrogel injected via TAE, (4) IDA@Gel TACE Group: 200 μL of 20 % Poloxamer-407 hydrogel gel containing 0.2 mg IDA was injected via TACE, (5) IF@Gel TACE Group: 200 μL of Fe_3O_4@ Gel composite hydrogel containing 0.2 mg IDA was injected via TACE.

Combination treatment for orthotopic HCC with abdominal metastasis: We divided a total of 20 rats into four treatment groups according to 5 rats/group: (1) Control group: no treatment; (2) IDA@Gel TACE Group: On day 0, TACE was performed via the hepatic artery with an injection of 200 μL of Fe_3O_4@Gel composite hydrogel containing 0.2 mg

IDA; (3) anti-PD-L1 group: anti-PD-L1 (10 mg/kg, based on rat body weight) was injected via tail vein on day 0, 3, and 6; (4) TACE + anti-PD-L1 Group: TACE was performed via hepatic artery on day 0, and 200 μL of IF@Gel was injected, and anti-PD-L1(10 mg/kg, based on rat body weight) was injected via tail vein on day 0, 3, and 6. Magnetic resonance was scanned for tumor progression before the start of treatment and on day 10 at the end point of treatment. Then, the survival rate of rats was counted up to day 40, during which the rats were euthanized if they showed cessation of water or food intake, malignant disease, etc., and were counted as dead.

2.9. Statistical analysis

Data were analyzed and processed using GraphPad Prism software (version 9.0.0), and all experiments were performed with at least three biological replications. Data were expressed as mean ± standard deviation (SD) and compared using one-way ANOVA, with $p < 0.05$ considered statistically significant.

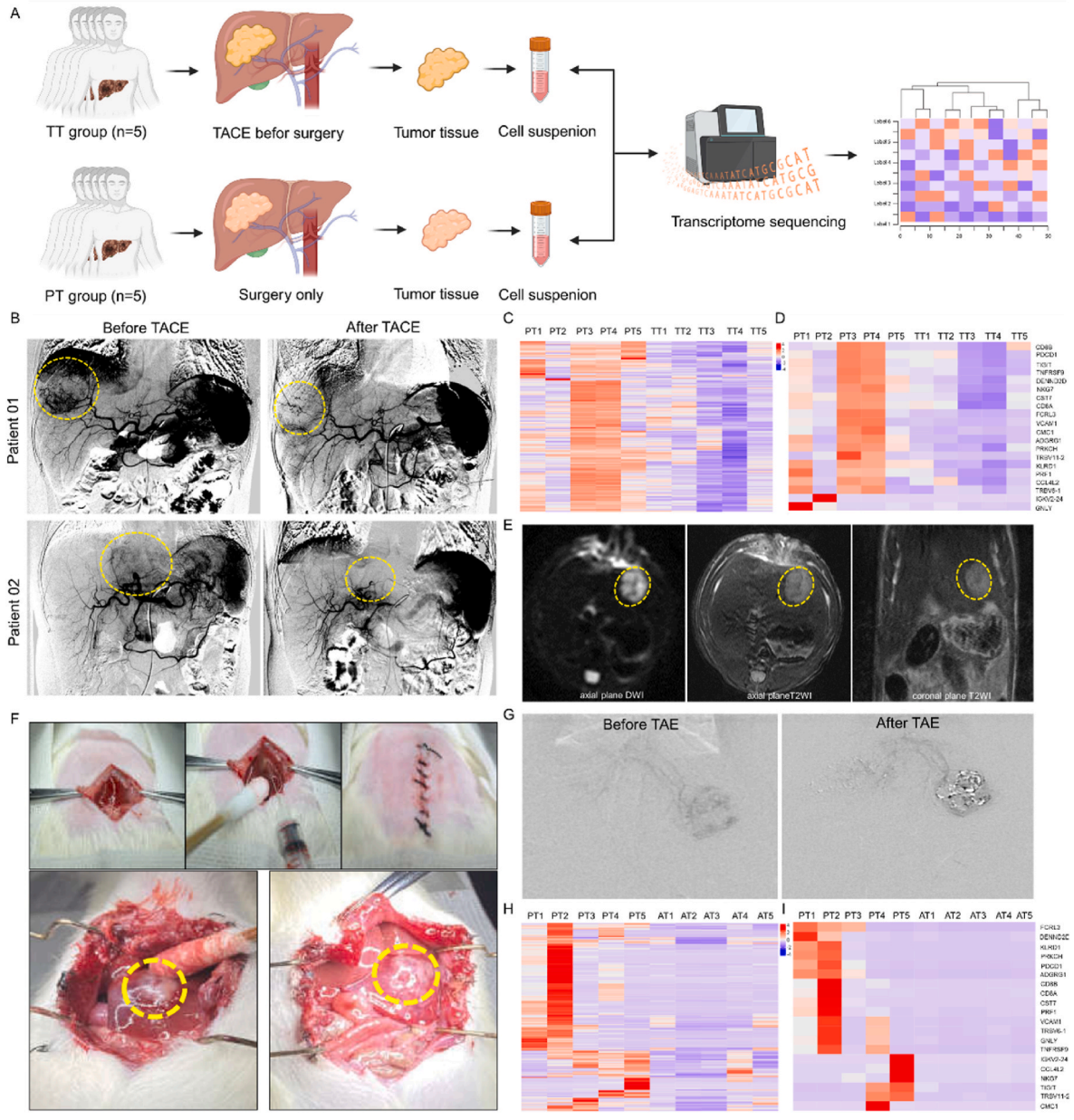

Fig. 1. Reduced $CD8^+$ T cell counts indicate an immunosuppressive microenvironment in clinical TACE cases and orthotopic HCC models in SD rats. (A) Schematic representation of the experimental strategy. PT: primary tumor; TT: TACE tumor. (B) Digital subtraction angiography (DSA) images of two HCC patients pre- and post-TACE. The photos show the disease sites, with yellow circled arrows indicating residual tumors with blood supply. (C) Differential gene expression of $CD8^+$ in HCC patient samples pre- and post-TACE sequencing. (D) Top 20 differentially expressed genes in HCC patient samples pre- and post-TACE sequencing. (E) Axial and coronal magnetic resonance imaging (MRI) scans were performed on SD rats with orthotopic HCC, using both diffusion-weighted imaging (DWI) and T2-weighted imaging (T2WI). (F) Construction process and results of the HCC rat model. A midline abdominal incision was made, and an insulin needle was used to puncture under the liver capsule, injecting N1S1 cell suspension into the liver. The incision was sutured, and tumor growth was re-examined by reopening the abdomen one week later. The yellow circle indicates the tumor. (G) DSA images of SD rats with orthotopic HCC pre- and post-TACE treatment. (H) Differential gene expression of $CD8^+$ in SD rat with orthotopic HCC samples pre- and post-TACE sequencing. (I) Top 20 differentially expressed genes in SD rat with orthotopic HCC samples pre- and post-TACE sequencing.

2.10. Materials, CCK-8 cytotoxicity assay, coagulation test, hemolysis assay, magnetic resonance imaging scan, HE staining, immunofluorescence staining, transcriptome sequencing, Western blotting, biochemical testing

The specifics of these procedures are outlined in the Supplementary Methods section.

3. Results and discussion

3.1. Reduced $CD8^+$ T cell counts indicate an immunosuppressive microenvironment in both clinical TACE cases and orthotopic HCC models in SD rats

In our clinical practice, conventional embolic agents like c-TACE and DEB-TACE are routinely used for HCC therapy to achieve arterial occlusion and induce ischemic necrosis in the tumor.However, TACE is significantly associated with a heightened probability of tumor recurrence and progression, with this unfavorable prognosis potentially attributable to the tumor immune microenvironment [12,23]. To explore this, we collected tumor samples from five untreated HCC patients and five patients treated with DEB-TACE (loaded with adriamycin) for transcriptome sequencing (Fig. 1A). The results revealed a differential expression of $CD8^+$−related genes (Fig. 1C), with the top 20 differentially expressed genes indicating a downregulation of $CD8^+$ expression in post-DEB-TACE patient samples (Fig. 1D). Notably, digital subtraction angiography (DSA) results from post-TACE patients demonstrated tumor size reduction and decreased blood supply (Fig. 1B).

To further investigate the underlying mechanisms, we established a highly feasible, simple, and effective orthotopic HCC rat research model using N1S1 cells to investigate the potential mechanisms further. In this model, SD rats were subcutaneously injected with N1S1 cell suspension via insulin needle puncture under the liver capsule through a midline abdominal incision. One week later, upon re-opening the abdomen, well-developed liver tumors were observed as single nodules with clear boundaries from the surrounding liver tissue, and no intrahepatic or abdominal metastases were detected (Fig. 1F). MRI scans on the 8th day post-tumor implantation revealed heterogeneous high signal intensity on T2-weighted imaging (T2WI) sequences (Fig. 1E). Histological examination and HE staining showed that the tumors were nodular, well-demarcated, encapsulated, and composed of poorly differentiated tumor cells with irregular polygonal shapes, deeply stained nuclei, and evidence of mitosis (Fig. S1). Arterial puncture and catheter insertion were successful when blood was aspirated from the syringe upon insertion or when the catheter was visibly filled with pulsatile blood, allowing a smooth infusion of physiological saline (Fig. S2). After injecting iodized oil through the syringe or microcatheter for embolization, partial liver lobes showed necrosis on the second-day post-procedure, indicating successful TAE intervention (Fig. S3).

Next, using the same method, we constructed an HCC rat model. Ten rats were divided into two groups: five untreated and five that underwent TACE using iodized oil. DSA imaging confirmed effective tumor embolization in the TACE group (Fig. 1G), and transcriptome sequencing results (Fig. 1H and I) aligned with human data.

The poor prognosis following TACE treatment may be associated with the tumor immune microenvironment, which has been shown to play a critical role in HCC recurrence [24]. Our study found that in clinical practice and orthotopic HCC rat models, conventional embolization materials induced an immune microenvironment characterized by a reduction in $CD8^+$ cells. The therapeutic efficacy of TACE is primarily determined by vascular occlusion caused by the embolic agents, the blockade of tumor blood supply, and the cytotoxic effects of chemotherapeutic drugs [25]. Among these, embolization is the most critical factor. TACE has become the first-line treatment for unresectable intermediate-stage liver cancer, mainly thanks to continuous improvements in embolization materials [26]. c-TACE employs super-liquid lipiodol as an embolic agent, supplemented with gelatin sponge particles. However, these materials have limitations. Lipiodol has weak embolization capabilities due to its rapid spread beyond the liver, while gelatin sponge particles are highly heterogeneous and handmade, leading to inconsistent embolization [27]. Additionally, the injection interval between lipiodol and the gelatin sponge can cause the spread of lipiodol and chemotherapeutic drugs beyond the liver, leading to systemic toxicity and reduced patient tolerance to anticancer drugs, thereby impacting treatment efficacy [28]. The advent of drug-eluting beads has further advanced TACE technology. These beads offer better embolization precision and controlled drug release, enhancing treatment safety and reducing adverse reactions [29]. However, their non-absorbable nature remains a limitation. Therefore, this study focuses on a critical aspect of TACE: the selection and improvement of pharmacological embolization materials and the mechanisms for improving immune microenvironmental suppression.

3.2. Preparation and characterization of biodegradable hydrogel IF@Gel

Given the immunomodulatory challenges posed by conventional embolic agents, we aim to design a biodegradable hydrogel and investigate whether its use leads to fewer immunological disruptions, thereby elucidating its mechanism of action.

To meet the criteria of easy preparation, biocompatibility, robust drug-loading, sustained drug release, and effective TACE embolization, we opted for Poloxamer-407 hydrogel as our carrier material (Fig. 2A). Poloxamer-407 is a polymeric nonionic surfactant composed of 70 % polyethylene oxide and 30 % polypropylene oxide. It exhibits temperature-sensitive behavior, transitioning from a sol to a gel state at its lower critical solution temperature (LCST), driven by hydrophobic-hydrophilic interactions between its components [30]. To enhance embolization duration and strength, we incorporated Fe_3O_4 nanoparticles (Fig. S4) into the hydrogel, forming Fe_3O_4@Gel. Idarubicin was chosen as the chemotherapeutic agent for incorporation into the hydrogel (IF@Gel) due to its higher cytotoxicity against HCC compared to other chemotherapeutic agents [31,32].

Characterization studies revealed that both Poloxamer-407 hydrogel and IF@Gel exhibited a flowing sol state at 4 °C but transitioned to a solid gel state at 37 °C and higher (Fig. 2B). The temperature-controlled phase transition process is remarkably smooth and rapid, with the sol-to-gel conversion occurring swiftly once the LCST was surpassed (Fig. 2C). Scanning electron microscopy (SEM) unveiled a highly porous and interconnected structure in IF@Gel (Fig. 2F and G), which was likely due to the increased cross-linking density from the Fe_3O_4 nanoparticles, resulting in reduced pore size and enhanced mechanical strength (Fig. 2D). In vitro degradation experiments demonstrated the degradation time of IF@Gel was significantly prolonged (Fig. S5). In vivo experiments in mice revealed that the IF@Gel degraded slowly under the skin and gradually spread into surrounding tissues, effectively releasing the drug over time (Fig. S6). In rat orthotopic HCC models, DSA imaging revealed incomplete embolization with Poloxamer-407 hydrogel, while IF@Gel effectively achieved embolization targets immediately and 2 h post-surgery (Fig. 2E). A series of biocompatibility tests, including CCK-8 cytotoxicity assays (Fig. 2H and I), coagulation tests (Fig. S7), and hemolysis assays (Figs. S8 and S9), demonstrated the excellent biocompatibility of Poloxamer-407 hydrogel and Fe_3O_4 nanoparticles. The CCK-8 assay showed that idarubicin exhibited significant cytotoxicity against rat N1S1 cells, with an IC50 value of 0.009 μg/mL after 24 h of exposure (Fig. 2J), consistent with previously reported values [31,32].

In our previous studies, Poloxamer-407 hydrogel demonstrated a very short degradation time, ranging from 15 min to 2 h, depending on its concentration. This duration is insufficient for effective tumor embolization. To address this, we modified it by incorporating Fe_3O_4 nanoparticle, an operationally simple and highly feasible method. The results confirmed the success of this modification, extending the

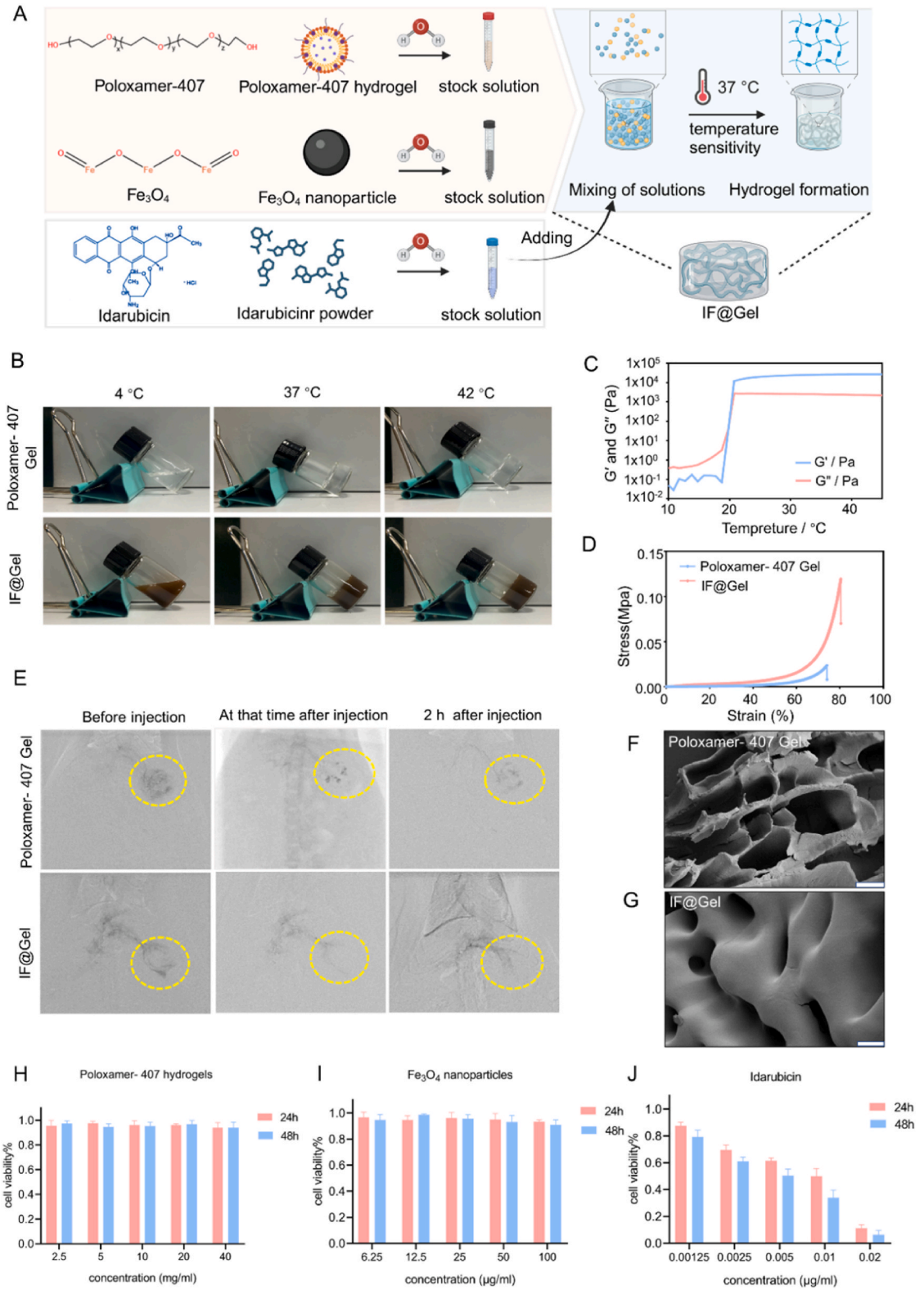

Fig. 2. Poloxamer-407 hydrogel and IF@Gel preparation and characterization. (A) Schematic diagram of hydrogel preparation. (B) Morphology of Poloxamer-407 hydrogel and IF@Gel at 4 °C, 37 °C, and 42 °C. (C) Frequency dependency of the elastic (G′) and viscous (G″) moduli of Poloxamer-407 hydrogel, its temperature-dependent rheological behavior. (D) Stress-strain curve of Poloxamer-407 hydrogel and IF@Gel. (E) TAE treatment of a rat orthotopic HCC model with DSA angiography (before TAE, immediately after TAE, and 2 h post-TAE) to observe embolization and degradation of Poloxamer-407 hydrogel and IF@Gel within the blood vessels. Yellow circles represent areas of embolization. (F) Scanning electron microscopy (SEM) observation of the morphology of Poloxamer-407 hydrogel. Scale bar 200 μm. (G) SEM observation of the morphology of IF@Gel. Scale bar 200 μm. (H ~ J) Co-culture of different concentration gradients of Poloxamer-407 Hydrogel (H), Fe_3O_4 nanoparticles (I), and IDA(J) with rat N1S1 cell line for 24 h and 48 h, followed by cell viability assessment using the CCK-8 assay. Data are mean ± SD (n = 3).

degradation time of the composite hydrogel to 6–12 h while enhancing its mechanical strength. This improvement brought the composite hydrogel closer to the ideal characteristics for biodegradable embolic materials. More importantly, Fe_3O_4 nanoparticles also provides excellent imaging assistance during imaging examinations, facilitating better tumor growth and treatment efficacy assessment.

Currently, there is no consensus on the optimal duration of embolization, defined as the time from embolic agent entry into the blood vessel to its degradation. Some embolic agents degrade in less than an hour [33], while others last for several months [34]. The former is inadequate for tumor treatment, while the latter can provoke substantial local inflammatory reactions and other adverse effects, disrupting the tumor microenvironment. Research suggests that a novel biodegradable microsphere that degrades within a few days can achieve ideal tumor treatment effects in animal models while inducing only mild local inflammatory reactions [35]. Most accepted biodegradable embolic materials degrade over several hours to days, a timeframe sufficient to induce tumor necrosis with minimal disturbance to the tumor microenvironment [36]. Our new Poloxamer-407 composite hydrogel is readily available, accessible to modify, and possesses good biocompatibility and drug release capabilities, achieving effective embolization. Therefore, our modification of the Poloxamer-407 hydrogel is relatively successful, and this composite material meets the requirements for further research.

3.3. *In vivo experiments on the therapeutic effect of IF@Gel for TAE/TACE in rats*

To assess the therapeutic efficacy of IF@Gel in TACE for HCC, 25 SD rats successfully constructed as in orthotopic HCC models were randomized into 5 groups and subjected to different treatments (refer to section 2.8 for details), followed by MRI monitoring of tumor growth and subsequent analysis of tumor tissues via histopathology, immunofluorescence, and RNA sequencing (Fig. 3A). The MRI indicates that, on the 10th day post-treatment, the most effective therapy was observed in the IF@Gel TACE group compared to the control group. In contrast, the Poloxamer-407 hydrogel TAE group exhibited the least favorable outcome (Fig. 3B and C). Among the remaining groups, the Fe_3O_4@Gel TAE group showed slightly superior efficacy to the IDA@Gel TACE group, emphasizing the importance of thorough embolization over chemotherapy agents. Moreover, in the Fe_3O_4@Gel and IF@Gel groups containing Fe_3O_4 nanoparticles, post-treatment MRI imaging displayed extremely low signal intensity in rat HCC tumors, indicating effective drug delivery into the tumor tissues.

Compared to the control group, HE staining of tumor tissues revealed areas of necrosis in all four treatment groups, with the most pronounced necrotic regions observed in the IF@Gel group, followed by the Fe_3O_4@Gel group (Fig. 3D). Furthermore, terminal deoxynucleotidyl transferase dUTP Nick-End labeling (TUNEL) immunofluorescence staining indicated that the IF@Gel group exhibited the highest number of apoptotic-stained cells, with the most vigorous fluorescence intensity (Fig. 3D and S10). Gene expression analysis of tumor tissues demonstrated significant differences in mRNA expression in all four treatment groups, indicating distinct molecular impacts of each treatment modality on the tumor (Fig. 3F).

Regarding safety, the biocompatibility and potential toxicity of IF@Gel were evaluated. There were no significant differences in body weight among the treatment groups of rats during the treatment period (Fig. 3E). Histopathological examination of major organs (heart, lungs, kidneys, intestines, and spleen) did not reveal any notable abnormalities (Fig. S11). Additionally, biochemical markers of liver and kidney function (alanine aminotransferase (ALT); aspartate transaminase (AST); creatinine (CREA); blood urea nitrogen (BUN)) remained within acceptable ranges (Fig. S12), indicating the favorable biocompatibility and absence of apparent toxicity of IF@Gel for TACE therapy.

Overall, the novel IDA-based Poloxamer-407 composite hydrogel TACE demonstrates significant therapeutic efficacy in treating orthotopic HCC in rats. Compared to the control group, tumor growth was inhibited in all treatment groups, with the most pronounced effect observed in the IF@Gel group. This indicates that our modifications to the Poloxamer-407 hydrogel were successful. The composite hydrogel effectively facilitated vascular embolization and sustained drug release, leading to apparent tumor suppression, apoptosis, and necrosis.

3.4. *Composite hydrogel for TACE treatment facilitates the balance between hypoxia and angiogenesis in the tumor microenvironment and alleviates the tumor immune microenvironment*

With the rapid growth of HCC cells, tumor tissues have an increased demand for nutrients and are in a hypoxic state. Vascular embolization therapy exacerbates this condition by restricting the blood supply, activating hypoxia-inducible factor (HIF-1α), which in turn triggers downstream responses such as angiogenesis, metabolism, autophagy, and apoptosis (Fig. 4A) [37,38]. These mechanisms create a risk of residual tumor cells, recurrence, and metastasis following TACE.

In our study, we explored the changes in hypoxia and angiogenesis within the tumor microenvironment after IF@Gel TACE treatment through genetic testing, Western blot, and immunofluorescence. We found that the higher the embolization intensity and the more severe the hypoxia, the more pronounced the activation of HIF- 1α (Fig. 4D and S 13A). Immunofluorescence assays revealed an increased fluorescence intensity of the vascular endothelial markers CD31 and CD34 in the Fe_3O_4@Gel and IF@Gel groups, suggesting that neo-angiogenesis occurred within the remaining tumor tissue, reflecting a dynamic stabilization of angiogenesis in response to embolization (Fig. 4D–S13B, and S13C). The expression of angiogenic factors (such as Pgf, Nrp1, Fgfr, Pdgfb, Pdgfc, Pdgfd, Pdgfra, and Pdgfrb) and anti-angiogenic factors (including Timp1, Notch1, Notch3, Notch4, Dll1, and Jag2) was also elevated, indicating activation of the angiogenic signaling pathway (Fig. 4C). Similarly, VEGF protein levels were upregulated (Fig. 4B). These findings suggest that angiogenic factor dynamics remained balanced at the current level of embolization intensity and duration.

This relatively mild response compared to traditional TACE is related to the shorter embolization time of the biodegradable hydrogel and the minimal foreign body reaction of the hydrogel within blood vessels and tumor tissues. Previous studies have confirmed that Poloxamer-407 hydrogel does not cause significant local inflammatory responses in blood vessels [39]. Inflammation is a negative factor in the tumor microenvironment, as inflammatory cells form an immunosuppressive environment, leading to immune evasion of tumor cells and promoting tumor progression [40].

Overexpression of VEGF within tumors can contribute to an immunosuppressive microenvironment by recruiting regulatory T cells, myeloid-derived suppressor cells, and immunosuppressive cytokines. This, in turn, inhibits dendritic cell maturation, suppresses T cell infiltration, and upregulates immune checkpoint expression on $CD8^+$ T cells [41,42]. To better understand the changes in the tumor microenvironment after IF@Gel TACE treatment, we conducted transcriptome sequencing to analyze the expression of immune-related genes. Our results showed that the expression of immune-related genes was upregulated to varying degrees in the four treatment groups that underwent hydrogel embolization, with relatively more pronounced expression in the IDA@Gel and IF@Gel groups and most significantly in the IF@Gel group (Fig. 4E). This suggested enhanced activation of cytotoxic T lymphocytes (CTLs) and natural killer (NK) cells, along with indications of potential negative feedback regulation on the anti-tumor immune response. RNA sequencing of tumor tissues from the IF@Gel group showed that the top 20 enriched pathways from the GO and KEGG analyses pointed to the activation of a complex anti-tumor immune response through multiple mechanisms (Fig. 4F and G). This immune response ultimately contributed to the attenuation of immunosuppression within the tumor microenvironment.

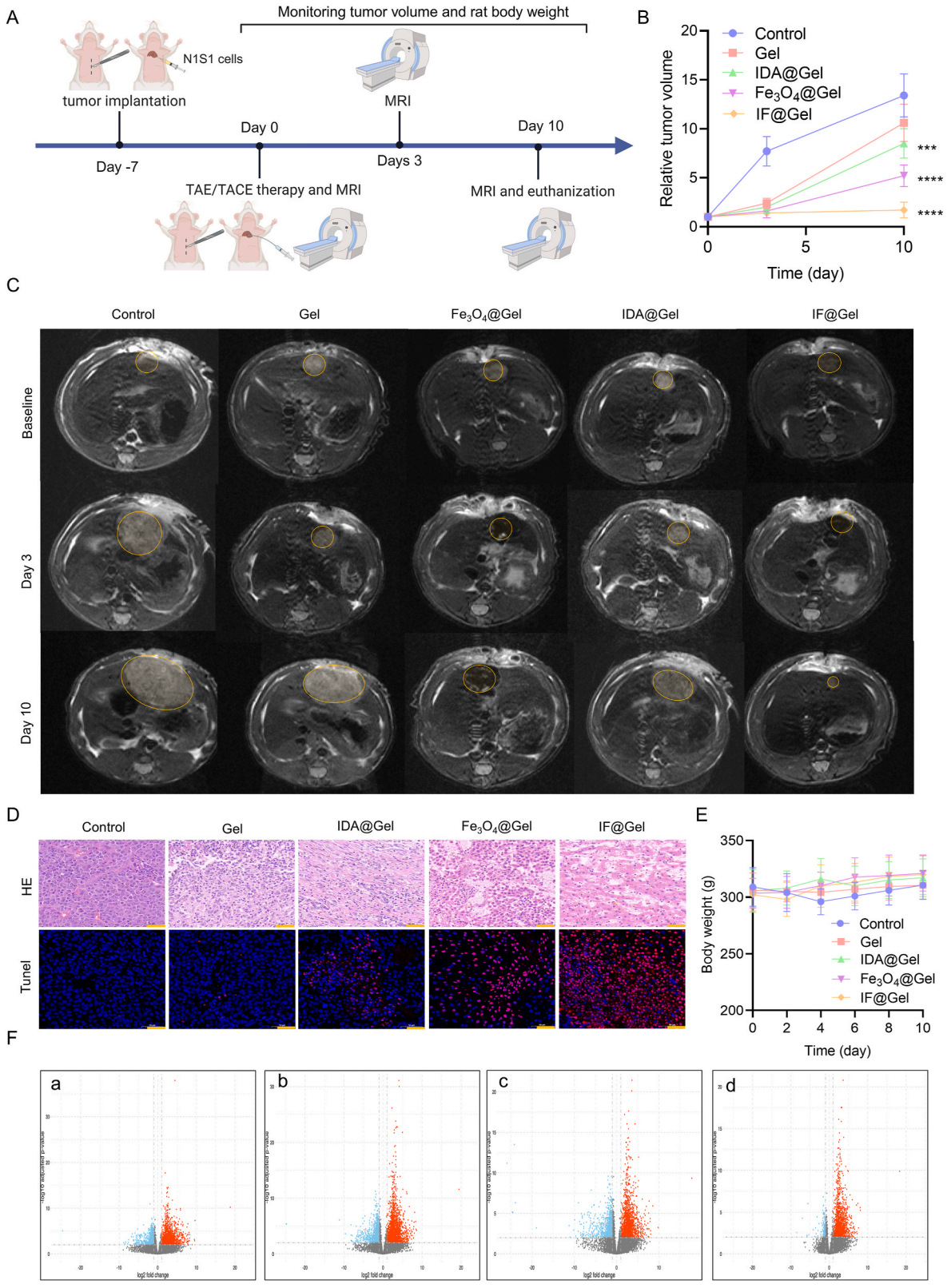

Fig. 3. IDA-based Fe_3O_4@Gel composite hydrogel for TACE treatment significantly inhibits orthotopic HCC in rats. (A) Schematic diagram of the treatment regimen. (B) Tumor volume was monitored in rats after TAE/TACE treatment using different therapies. Data are mean ± SD (n = 5). (C) Tumor images of rats undergoing TAE/TACE treatment on days 0, 3, and 10, as observed through MRI scans with T2WI sequence. The photos chosen represent the slice with the largest tumor diameter. Yellow circles indicate the tumor. (D) HE-stained histopathological sections and TUNEL immunofluorescence staining of rats 10 days after receiving different TAE/TACE treatments. Scale bar: 50 μm. (E) The body weights of rats were monitored after TAE/TACE treatment using different therapies. Data are mean ± SD (n = 5). (F) Transcriptome sequencing shows the expression of differentially expressed genes in treatment groups Gel (a), Fe_3O_4@Gel (b), IDA@Gel (c), and IF@Gel (d) compared to the control group.

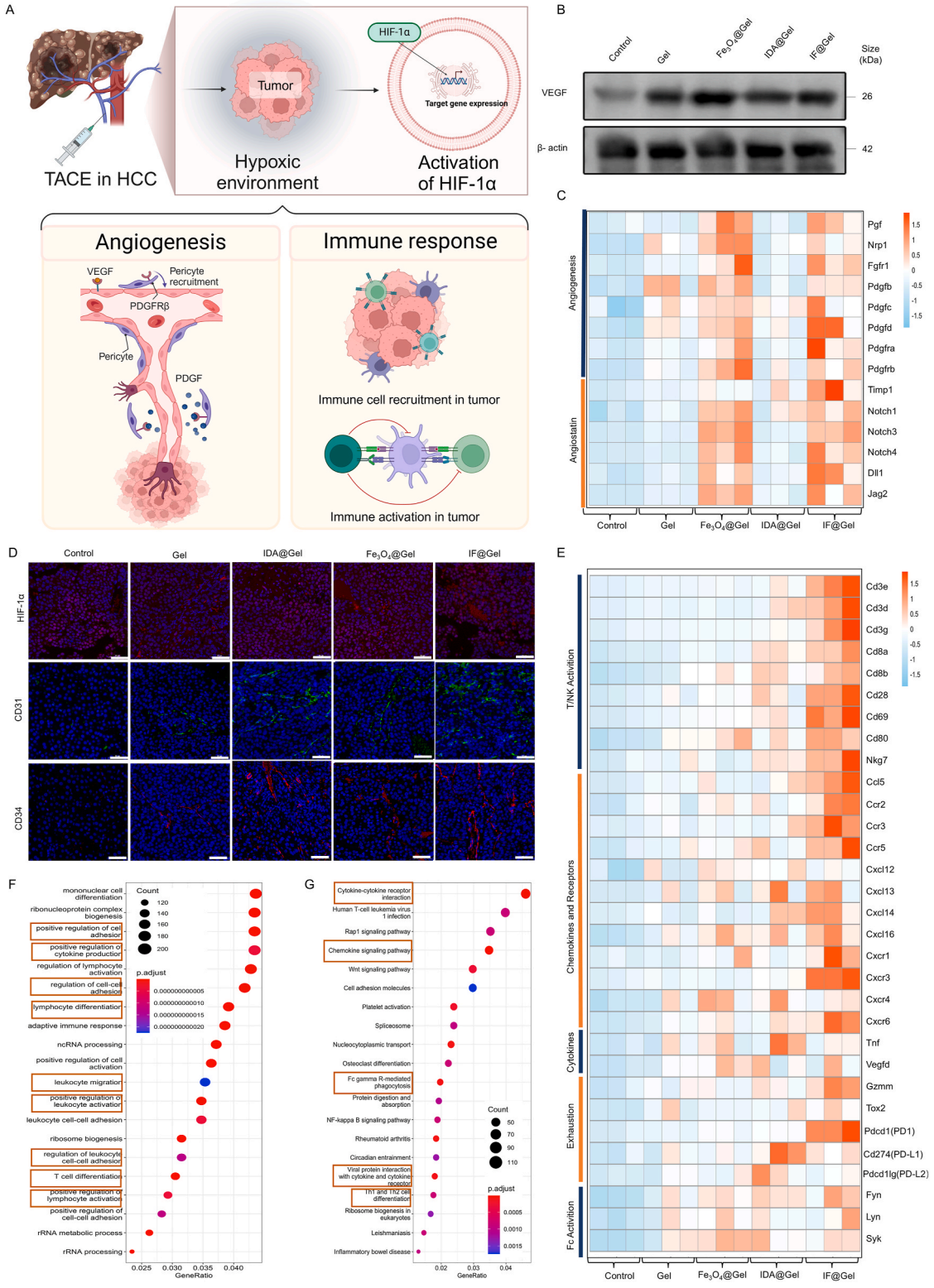

Fig. 4. Composite hydrogel for TACE treatment facilitates the balance between hypoxia and angiogenesis in the tumor microenvironment and alters the immune microenvironment. (A) Schematic diagram showing hypoxia, angiogenesis, and immune microenvironment changes in the tumor microenvironment after TACE treatment with IF@Gel. (B) Western blot analysis of VEGF expression in tumor tissues of orthotopic HCC rats from different groups after ten days of different TAE/TACE treatments. (C) Transcriptome sequencing analysis of the expression of hypoxia-inducible factors and angiogenesis-related genes in tumor tissues of orthotopic HCC rats from different groups after ten days of different TAE/TACE treatments, with red indicating gene upregulation. (D) Fluorescence intensity of HIF-1α and endothelial cell markers CD31 and CD34 observed under a fluorescence microscope. Scale bar, 50 μm. (E) Transcriptome sequencing analysis of the expression of T/NK cells, cytokines, and chemokines-related genes in tumor tissues of orthotopic HCC rats from different groups after ten days of different TAE/TACE treatments, with red indicating gene upregulation. (F, G) GO and KEGG enrichment analyses show the top 20 enriched pathways in tumor tissues of the IF@Gel treatment group, with immune-related pathways highlighted in red boxes.

Some studies have reported that TAE results in the upregulation of only a limited number of immune cells, without triggering widespread immune activation [43,44]. The degradation of the hydrogel within the blood vessels, leading to partial restoration of blood supply, may facilitate immune cell infiltration. However, our research revealed that using hydrogel as an embolization material in TACE upregulated the expression of anti-tumor immune-related genes. Notably, the TACE group treated with IDA exhibited stronger immune activation compared to the drug-free TAE group. Therefore, we hypothesize that IDA, as a DNA-damaging agent, may induce ICD through DNA damage response (DDR), further activating and enhancing anti-tumor immunity [45].

3.5. *IDA-loading hydrogels activate ICD and synergize with anti-PD-L1 therapy for antitumor immunity*

In the previous section, we found that IDA-loaded hydrogels were more effective in anti-tumor immune activation. Therefore, we speculate that IDA, as a DNA-damaging drug, may have induced ICD, which

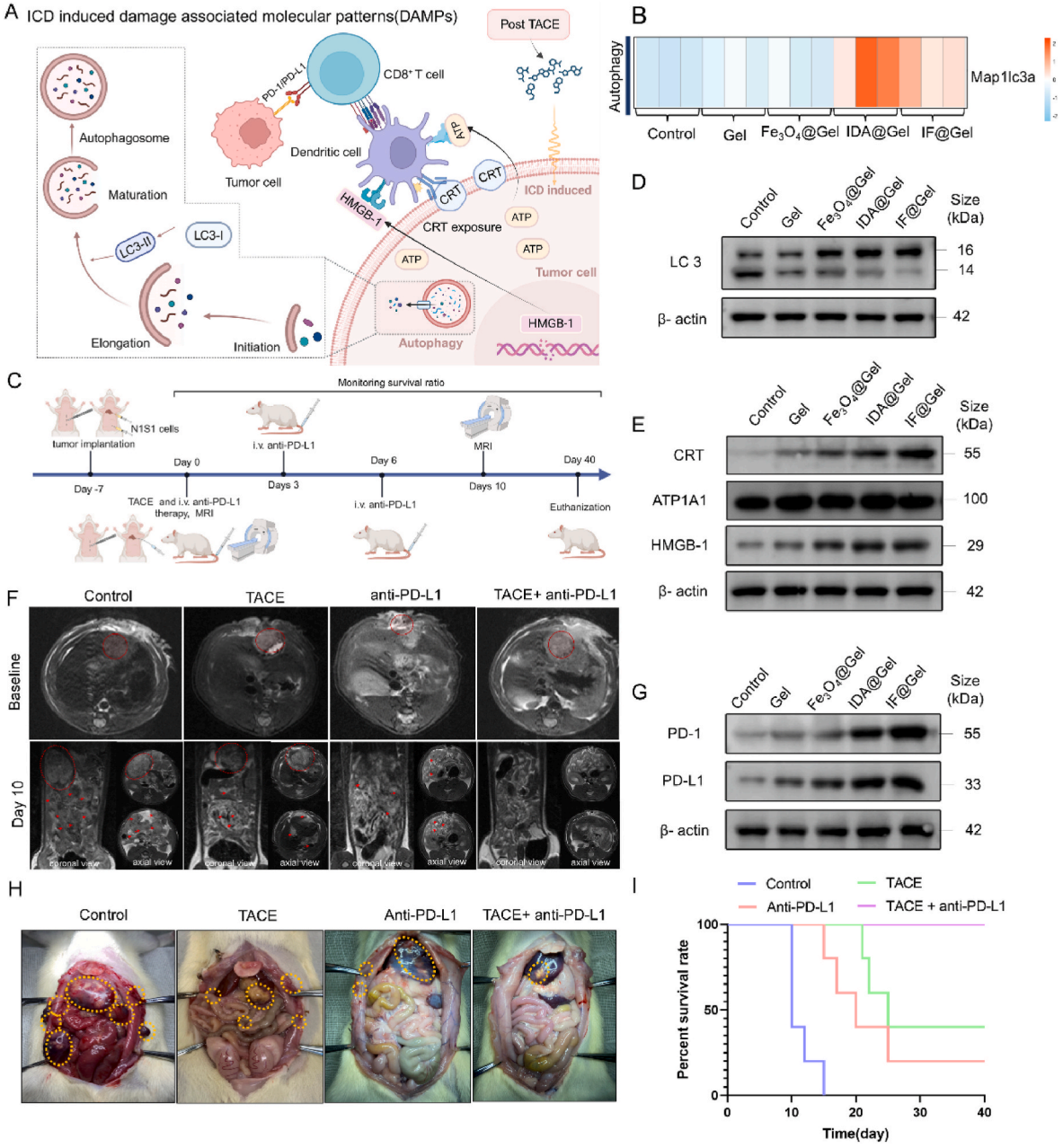

Fig. 5. IDA-loading hydrogels activate ICD and synergize with anti-PD-L1 therapy for antitumor immunity. (A) Schematic diagram illustrating the ICD effect of IF@Gel after TACE treatment. (B) Expression of autophagy marker genes in transcriptome sequencing of orthotopic HCC rats from different groups after ten days of different TAE/TACE treatments. n = 5 (C) Schematic diagram of the treatment regimen for orthotopic HCC rats with peritoneal metastasis of liver cancer cells using IF@Gel combined with anti-PD-L1 therapy. (D) Western blot analysis of autophagy-related protein expression in tumor tissues of orthotopic HCC rats from different groups after ten days of different TAE/TACE treatments. (E) Western blot analysis of the expression of immunogenic cell death marker proteins CRT and HMGB1 in tumor tissues of orthotopic HCC rats from different groups after ten days of different TAE/TACE treatments. (F) MRI monitoring of tumor progression in different treatment groups of IF@Gel combined with anti-PD-L1 after TACE treatment immediately and on the 10th day post-treatment. Red circles indicate tumor size. n = 5. (G) Western blot analysis of the expression of PD-1 and PD-L1 proteins in tumor tissues of orthotopic HCC rats from different groups after ten days of different TAE/TACE treatments. (H) Evaluation of tumor and ascites status on the 40th day of TACE combined treatment with IF@Gel and anti-PD-L1 therapy in different treatment groups. (I) Survival analysis of rats treated with TACE combined with IF@Gel and anti-PD-L1 therapy. n = 5.

further activated and enhanced anti-tumor immunity (Fig. 5A). High mobility group box-1 protein (HMGB1) release and calreticulin (CRT) exposure are the gold standard for accurately predicting the ability of chemotherapeutic agents to induce apoptosis [46]. To confirm this, we performed a Western blot assay, which revealed increased expression of both HMGB1 and CRT proteins (Fig. 5E), thereby validating ICD activation.

Another feature of the ICD response is the activation of autophagy [47]. Autophagy-driven ICD mechanisms may play a central role in regulating the secretion and degradation of HMGB1 [48]. We examined the expression of autophagy marker LC3 using protein blotting and found that autophagy activation was consistently observed at both the gene and protein levels (Fig. 5B and D). The up-regulation of autophagy levels after TACE, especially after adding IDA to the treatment, suggests a positive correlation between autophagy and the induction of ICD.

Additionally, we found that ICD activation was accompanied by upregulation of PD-1 and PD-L1 protein expression (Fig. 4E and 5G). As is well-known, PD-1/PD-L1 is an essential immune checkpoint molecule that plays a vital role in maintaining peripheral immune tolerance and suppressing the body's anti-tumor immunity [4,49]. Given this, we hypothesized that combining anti-PD-L1 (BioXcell, BE0383), an immune checkpoint inhibitor (ICI), with ICD activation could lead to enhanced anti-tumor immune responses. To test this, we used a rat model of orthotopic HCC with abdominal metastasis and divided the animals into four treatment groups (see section 2.8 for details). Tumor progression was monitored via MRI, and the survival rate of the rats was tracked for 40 days (Fig. 5C). By the 10th day, the control group exhibited the most severe primary tumor and abdominal metastasis, along with the most significant amount of ascites (Fig. 5H). In contrast, the group treated with TACE-loaded IDA composite hydrogel combined with anti-PD-L1 injection displayed the best outcomes (Fig. 5H). MRI scans and laparotomies revealed no significant abdominal metastases and only a small amount of ascites (Fig. 5F). Within the observation period of 40 days for survival analysis, all rats in the combined treatment group survived, indicating the excellent efficacy of the combined treatment (Fig. 5I). These findings highlight the strong potential of this combined approach in enhancing anti-tumor immunity and improving treatment outcomes.

4. Conclusion

In conclusion, we employed TACE with a novel Poloxamer-407 composite hydrogel loaded with IDA to evaluate its therapeutic efficacy in an orthotopic HCC model in SD rats. We also explored the alterations in the tumor immune microenvironment following treatment and investigated the potential role of ICD in these processes. The Poloxamer-407 hydrogel, combined with Fe_3O_4 nanoparticles, demonstrated an optimal degradation rate, suitable mechanical strength, high biocompatibility, effective drug-loading capacity, and sustained-release properties, making it a promising candidate for use as a TACE embolic material. Our findings showed that IF@Gel-based TACE provided strong therapeutic efficacy in the orthotopic HCC model, and ICD activation could synergize with anti-PD-L1 therapy by enhancing anti-tumor immunity. This study underscores the role of ICD in HCC, particularly within this treatment strategy, and sheds light on its potential mechanisms—especially regarding modulation of the tumor immune microenvironment following TACE. These insights offer a new perspective on the classification and precision treatment of HCC, as well as its combination with ICIs.

CRediT authorship contribution statement

Xiaokai Zhang: Writing – original draft, Visualization, Validation, Project administration, Methodology, Investigation, Formal analysis, Data curation. **Xiujiao Deng:** Writing – original draft, Methodology, Investigation, Formal analysis, Data curation. **Jizhou Tan:** Writing – original draft, Visualization, Methodology, Formal analysis, Data curation, Conceptualization. **Haikuan Liu:** Methodology, Investigation, Data curation. **Hong Zhang:** Visualization, Methodology. **Chengzhi Li:** Visualization, Validation, Investigation, Conceptualization. **Qingjun Li:** Methodology. **Jinxue Zhou:** Writing – review & editing, Supervision, Resources, Project administration, Funding acquisition, Conceptualization. **Zeyu Xiao:** Writing – review & editing, Supervision, Resources, Project administration, Methodology, Data curation, Conceptualization. **Jiaping Li:** Writing – review & editing, Supervision, Resources, Project administration, Funding acquisition, Data curation, Conceptualization.

Declaration of competing interest

The authors declare that there are no conflicts of interest regarding the publication of this manuscript. The research presented in this paper was conducted independently, without any financial or personal relationships that could be perceived to influence the work reported in this study.

The authors have no commercial or financial involvement with any organizations that could be seen as having an interest in the outcomes of this research. All funding sources supporting this work have been appropriately acknowledged within the manuscript.

Acknowledgments

We acknowledge funding by the Guangdong Basic and Applied Basic Research Foundation (2023A1515012660,2022A1515220159 and 2023A1515220128), Medical Joint Fund of Jinan University (YXJC2022008), Clinical characteristic technology projects in Guangzhou City (C3230118), the National Natural Science Foundation of China (82271943, 82172036 and 82372059), the Science and Technology Development Foundation of Henan Province (242102311180). Figures were created with BioRender.com.

Appendix A. Supplementary data

Supplementary data to this article can be found online at https://doi.org/10.1016/j.mtbio.2024.101343.

Data availability

Data will be made available on request.

References

[1] A. Vogel, et al., Hepatocellular carcinoma, Lancet 400 (10360) (2022) 1345–1362.
[2] S.M. Yoon, et al., Efficacy and safety of transarterial chemoembolization plus external beam radiotherapy vs sorafenib in hepatocellular carcinoma with macroscopic vascular invasion: a randomized clinical trial, JAMA Oncol. 4 (5) (2018) 661–669.
[3] J.M. Llovet, et al., Hepatocellular carcinoma, Nat. Rev. Dis. Prim. 7 (1) (2021) 6.
[4] Y. Chao, et al., Localized cocktail chemoimmunotherapy after in situ gelation to trigger robust systemic antitumor immune responses, Sci. Adv. 6 (10) (2020) eaaz4204.
[5] EASL clinical practice guidelines: management of hepatocellular carcinoma, J. Hepatol. 69 (1) (2018) 182–236.
[6] J.M. Llovet, et al., Arterial embolisation or chemoembolisation versus symptomatic treatment in patients with unresectable hepatocellular carcinoma: a randomised controlled trial, Lancet 359 (9319) (2002) 1734–1739.
[7] D. Xia, et al., Lenvatinib with or without concurrent drug-eluting beads transarterial chemoembolization in patients with unresectable, advanced hepatocellular carcinoma: a real-world, multicenter, retrospective study, Liver Cancer 11 (4) (2022) 368–382.
[8] H.Y. Woo, J. Heo, Transarterial chemoembolization using drug eluting beads for the treatment of hepatocellular carcinoma: now and future, Clin. Mol. Hepatol. 21 (4) (2015) 344–348.
[9] M. Chen, et al., HIF-2α-targeted interventional chemoembolization multifunctional microspheres for effective elimination of hepatocellular carcinoma, Biomaterials 284 (2022) 121512.
[10] J.Q. Li, et al., Hypoxia induces universal but differential drug resistance and impairs anticancer mechanisms of 5-fluorouracil in hepatoma cells, Acta Pharmacol. Sin. 38 (12) (2017) 1642–1654.

[11] M. Potente, H. Gerhardt, P. Carmeliet, Basic and therapeutic aspects of angiogenesis, Cell 146 (6) (2011) 873–887.
[12] Y. Sun, et al., Single-cell landscape of the ecosystem in early-relapse hepatocellular carcinoma, Cell 184 (2) (2021) 404–421.e16.
[13] J. Tan, et al., TREM2(+) macrophages suppress CD8(+) T-cell infiltration after transarterial chemoembolisation in hepatocellular carcinoma, J. Hepatol. 79 (1) (2023) 126–140.
[14] A. Schicho, et al., Impact of different embolic agents for transarterial chemoembolization (TACE) procedures on systemic vascular endothelial growth factor (VEGF) levels, J Clin Transl Hepatol 4 (4) (2016) 288–292.
[15] R. Minici, et al., Safety and efficacy of degradable starch microspheres transcatheter arterial chemoembolization as a bridging therapy in patients with early stage hepatocellular carcinoma and child-pugh stage B eligible for liver transplant, Front. Pharmacol. 12 (2021) 634084.
[16] Z. Zheng, et al., Idarubicin-loaded biodegradable microspheres enhance sensitivity to anti-PD1 immunotherapy in transcatheter arterial chemoembolization of hepatocellular carcinoma, Acta Biomater. 157 (2023) 337–351.
[17] Q.J. Li, et al., Hepatic arterial infusion of oxaliplatin, fluorouracil, and leucovorin versus transarterial chemoembolization for large hepatocellular carcinoma: a randomized phase III trial, J. Clin. Oncol. 40 (2) (2022) 150–160.
[18] D.V. Krysko, et al., Immunogenic cell death and DAMPs in cancer therapy, Nat. Rev. Cancer 12 (12) (2012) 860–875.
[19] Y. Sun, et al., Immunogenicity and cytotoxicity of a platinum(IV) complex derived from capsaicin, Dalton Trans. 50 (10) (2021) 3516–3522.
[20] H. Zhu, et al., Oxaliplatin induces immunogenic cell death in hepatocellular carcinoma cells and synergizes with immune checkpoint blockade therapy, Cell. Oncol. 43 (6) (2020) 1203–1214.
[21] Y. Xue, et al., Platinum-based chemotherapy in combination with PD-1/PD-L1 inhibitors: preclinical and clinical studies and mechanism of action, Expet Opin. Drug Deliv. 18 (2) (2021) 187–203.
[22] D.J. Pinato, et al., Trans-arterial chemoembolization as a loco-regional inducer of immunogenic cell death in hepatocellular carcinoma: implications for immunotherapy, J Immunother Cancer 9 (9) (2021).
[23] D.H. Palmer, K. Malagari, L.M. Kulik, Role of locoregional therapies in the wake of systemic therapy, J. Hepatol. 72 (2) (2020) 277–287.
[24] L. Li, et al., Radiofrequency-responsive dual-valent gold nanoclusters for enhancing synergistic therapy of tumor ablation and artery embolization, Nano Today 35 (2020) 100934.
[25] D. Wang, W. Rao, Bench-to-bedside development of multifunctional flexible embolic agents, Theranostics 13 (7) (2023) 2114–2139.
[26] C. Aliberti, et al., Transarterial chemoembolization with small drug-eluting beads in patients with hepatocellular carcinoma: experience from a cohort of 421 patients at an Italian center, J Vasc Interv Radiol 28 (11) (2017) 1495–1502.
[27] R. Lencioni, et al., Lipiodol transarterial chemoembolization for hepatocellular carcinoma: a systematic review of efficacy and safety data, Hepatology 64 (1) (2016) 106–116.
[28] J. Zeng, et al., Radiopaque and uniform alginate microspheres loaded with tantalum nanoparticles for real-time imaging during transcatheter arterial embolization, Theranostics 8 (17) (2018) 4591–4600.
[29] M. Burrel, et al., Survival of patients with hepatocellular carcinoma treated by transarterial chemoembolisation (TACE) using Drug Eluting Beads. Implications for clinical practice and trial design, J. Hepatol. 56 (6) (2012) 1330–1335.
[30] B. Jeong, S.W. Kim, Y.H. Bae, Thermosensitive sol-gel reversible hydrogels, Adv. Drug Deliv. Rev. 54 (1) (2002) 37–51.
[31] L. Marelli, et al., Transarterial therapy for hepatocellular carcinoma: which technique is more effective? A systematic review of cohort and randomized studies, Cardiovasc. Intervent. Radiol. 30 (1) (2007) 6–25.
[32] P.R. Galle, et al., EASL clinical practice guidelines: management of hepatocellular carcinoma, J. Hepatol. 69 (1) (2018) 182–236.
[33] S.Y. Lee, et al., Hyaluronic acid/doxorubicin nanoassembly-releasing microspheres for the transarterial chemoembolization of a liver tumor, Drug Deliv. 25 (1) (2018) 1472–1483.
[34] T. Yamasaki, et al., Effect of transcatheter arterial infusion chemotherapy using iodized oil and degradable starch microspheres for hepatocellular carcinoma, J. Gastroenterol. 47 (6) (2012) 715–722.
[35] R.J. Owen, et al., A preclinical study of the safety and efficacy of Occlusin™ 500 Artificial Embolization Device in sheep, Cardiovasc. Intervent. Radiol. 35 (3) (2012) 636–644.
[36] Z. Li, et al., Smart nanotherapeutic targeting of tumor vasculature, Acc. Chem. Res. 52 (9) (2019) 2703–2712.
[37] S.H. Choi, et al., Knockdown of HIF-1α and IL-8 induced apoptosis of hepatocellular carcinoma triggers apoptosis of vascular endothelial cells, Apoptosis 21 (1) (2016) 85–95.
[38] Y. Chao, Z. Liu, Biomaterials tools to modulate the tumour microenvironment in immunotherapy, Nature Reviews Bioengineering 1 (2) (2023) 125–138.
[39] M. Boodhwani, et al., Effects of purified poloxamer 407 gel on vascular occlusion and the coronary endothelium, Eur. J. Cardio. Thorac. Surg. 29 (5) (2006) 736–741.
[40] G.P. Dunn, L.J. Old, R.D. Schreiber, The three Es of cancer immunoediting, Annu. Rev. Immunol. 22 (2004) 329–360.
[41] J.E. Ohm, et al., VEGF inhibits T-cell development and may contribute to tumor-induced immune suppression, Blood 101 (12) (2003) 4878–4886.
[42] T. Voron, et al., VEGF-A modulates expression of inhibitory checkpoints on CD8+ T cells in tumors, J. Exp. Med. 212 (2) (2015) 139–148.
[43] U. Stampfl, et al., Experimental liver embolization with four different spherical embolic materials: impact on inflammatory tissue and foreign body reaction, Cardiovasc. Intervent. Radiol. 32 (2) (2009) 303–312.
[44] V. Verret, et al., Influence of degradation on inflammatory profile of polyphosphazene coated PMMA and trisacryl gelatin microspheres in a sheep uterine artery embolization model, Biomaterials 32 (2) (2011) 339–351.
[45] A.D. Garg, et al., Trial watch: immunogenic cell death induction by anticancer chemotherapeutics, OncoImmunology 6 (12) (2017) e1386829.
[46] J. Zhou, et al., Immunogenic cell death in cancer therapy: present and emerging inducers, J. Cell Mol. Med. 23 (8) (2019) 4854–4865.
[47] M. Michaud, et al., Autophagy-dependent anticancer immune responses induced by chemotherapeutic agents in mice, Science 334 (6062) (2011) 1573–1577.
[48] W. Hou, et al., Strange attractors: DAMPs and autophagy link tumor cell death and immunity, Cell Death Dis. 4 (12) (2013) e966.
[49] M. Yi, et al., Combination strategies with PD-1/PD-L1 blockade: current advances and future directions, Mol. Cancer 21 (1) (2022) 28.